

# Search for 511 keV Emission in Satellite Galaxies of the Milky Way with INTEGRAL/SPI

Thomas Siegert<sup>1\*</sup>, Roland Diehl<sup>1,2</sup>, Aaron C. Vincent<sup>3</sup>, Fabrizia Guglielmetti<sup>1,4</sup>, Martin G. H. Krause<sup>5</sup>, and Celine Boehm<sup>3</sup>

<sup>1</sup> Max-Planck-Institut für extraterrestrische Physik, Gießenbachstraße, D-85741 Garching, Germany

<sup>2</sup> Excellence Cluster Universe, Boltzmannstraße 2, D-85748, Garching, Germany

<sup>3</sup> Institute for Particle Physics Phenomenology, Department of Physics, Durham University, Durham DH1 3LE, United Kingdom

<sup>4</sup> Max-Planck-Institut für Astrophysik, Karl-Schwarzschild-Straße 1, D-85748 Garching, Germany

<sup>5</sup> School of Physical Sciences, University of Tasmania, Hobart, TAS, 7005, Australia

Received 17 Jun 2016 / Accepted 30 Jul 2016

## ABSTRACT

**Context.** The positron ( $e^+$ ) annihilation  $\gamma$ -ray signal in the Milky Way (MW) shows a puzzling morphology: a very bright bulge and a very low surface-brightness disk. A coherent explanation of the  $e^+$  origin, propagation through the Galaxy and subsequent annihilation in the interstellar medium has not yet been found. Tentative explanations involve  $e^+$ s from radioactivity, X-ray binaries, and dark matter (DM).

**Aims.** Dwarf satellite galaxies (DSGs) are believed to be DM-dominated and hence are promising candidates in the search for 511 keV emission as a result of DM annihilation into  $e^+e^-$ -pairs. The goal of this study is to constrain possible 511 keV  $\gamma$ -ray signals from 39 DSGs of the MW and to test the annihilating DM scenario.

**Methods.** We use the spectrometer SPI on INTEGRAL to extract individual spectra for the studied objects in the range 490–530 keV. As the diffuse galactic 511 keV emission dominates the overall signal, the large scale morphology of the MW has been modelled accordingly and was included in a maximum likelihood analysis. Alternatively, a distance-weighted stacked spectrum has been determined, representing an average DSG seen in 511 keV.

**Results.** Only Reticulum II (Ret II) shows a  $3.1\sigma$  signal. Five other sources show tentative  $2\sigma$  signals. The mass-to-511 keV luminosity-ratio,  $\Upsilon_{511}$ , shows a marginal trend towards higher values for intrinsically brighter objects, opposite to the mass-to-light-ratio,  $\Upsilon_V$  in the V-band, which is generally used to uncover DM in DSGs.

**Conclusions.** All derived 511 keV flux values or upper limits are above the flux level implied by a DM interpretation of the MW bulge signal. The signal detected from Ret II is unlikely to be related to a DM origin alone, otherwise, the MW bulge would be  $\sim 100$  times brighter in 511 keV than what is seen with SPI. Ret II is exceptional considering the DSG sample, and rather points to enhanced recent star formation activity, if its origins are similar to processes in the MW. Understanding this emission may provide further clues regarding the origin of the annihilation emission in the MW bulge.

**Key words.** Positrons, Gamma rays: general, ISM: general, Galaxies: dwarf satellites, Techniques: spectroscopic, Cosmology: dark matter

## 1. Introduction

It has been proposed that the 511 keV morphology of the Milky Way (MW), originating in the annihilation of electrons ( $e^-$ s) with positrons ( $e^+$ s), seen by INTEGRAL (Winkler et al. 2003), could be related to the decay or annihilation of dark matter (DM) particles (Hooper et al. 2004; Ascasibar et al. 2006). From theoretical considerations it was suggested that when light DM particles ( $1 \text{ MeV } c^{-2} \lesssim m_\chi \lesssim 100 \text{ MeV } c^{-2}$ ) annihilate or decay, they could produce  $e^+$ s with low kinetic energies of  $\sim \text{MeV}$  (Boehm et al. 2004; Hooper et al. 2004; Picciotto & Pospelov 2005; Beacom & Yüksel 2006; Gunion et al. 2006; Pospelov et al. 2008; Boehm & Silk 2008). The annihilation of these  $e^+$ s with  $e^-$ s from the interstellar medium (ISM) would lead to the signature that was measured by the spectrometer SPI (Vedrenne et al. 2003) on INTEGRAL.

The galactic diffuse large-scale 511 keV emission that was measured with balloon-flight experiments (e.g. Leventhal et al.

1978) and with SPI (Knödlseder et al. 2005; Bouchet et al. 2010; Skinner et al. 2014) was found to be concentrated towards the bulge region of the MW, reminiscent of a DM halo profile. However, other – less exotic – sources may also explain this signal (see Prantzos et al. 2011, for a review).

If the entire bulge annihilation radiation originates from DM particles, the apparently DM-dominated dwarf satellite galaxies (DSGs) of the MW should also emit a measurable 511 keV signal (Hooper et al. 2004; Simon & Geha 2007; Strigari et al. 2008b). Based on cold dark matter (CDM) cosmology and the corresponding galaxy formation model (see e.g. White & Rees 1978; Springel et al. 2005; Moster et al. 2013), the satellite galaxies of the MW must be DM-dominated (Mateo 1998; Strigari et al. 2008a; McConnachie 2012).

A good test of the annihilating DM hypothesis is thus to check in cumulative INTEGRAL data for a consistent 511 keV brightness from the known satellites of the MW, depending on their DM content and distance. Cordier et al. (2004) tested this for the case of the Sagittarius Dwarf Spheroidal (Sag). A point-like emission, as expected from DM annihilation (see below),

\* E-mail: tsiegert@mpe.mpg.de

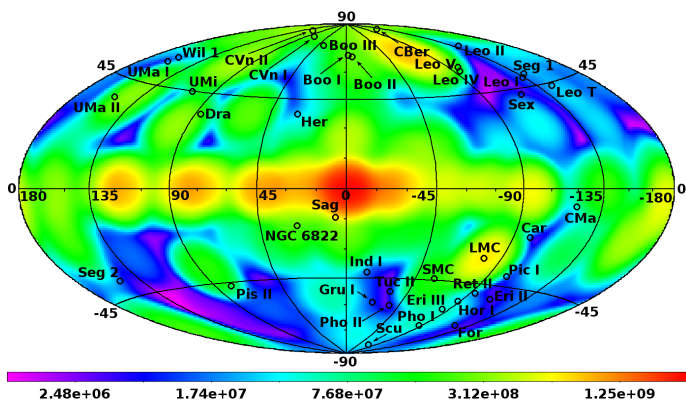


Fig. 1: Sky exposure with SPI after 1258 orbits of the INTEGRAL mission. Tested satellite galaxies of the Milky Way are marked with a circle. Colourbar shows the SPI exposure in units of  $\text{cm}^2 \text{s}$ . The effective area of SPI at photon energies of 511 keV is  $\approx 75 \text{ cm}^2$ .

could not be detected, and a  $2\sigma$  upper limit on the 511 keV flux of  $2.5 \times 10^{-4} \text{ ph cm}^{-2} \text{ s}^{-1}$  was established. They could neither exclude nor corroborate DM as the cause of the 511 keV emission in the MW because the upper limit from Sag compared to the MW bulge flux was not constraining enough. However, this is based on the assumption that the whole 511 keV emission in the bulge of the MW arises from annihilating DM.

In this work, we extend and refine these previous studies, using more than ten years of INTEGRAL/SPI data covering the full sky. We report a new search for point-like 511 keV line emission at the positions of 39 DSGs of the MW within 500 kpc in order to provide new constraints on a DM origin of the galactic positron signal. We also report on the discovery of a tentative signal in the Reticulum II dwarf galaxy.

## 2. Data and their Analysis

### 2.1. Data Set, Background Model, and Celestial Large-Scale Emission

The data that we analysed in this work were taken between 12 Dec 2002 and 7 Apr 2013 with the spectrometer SPI on ESA’s INTEGRAL satellite, and are identical to the data set of Siegert et al. (2016, hereafter Paper I). Therefore, we refer to this paper for detailed information on the data selection and analysis procedure.

In total, 73590 pointings with an overall exposure time of 160 Ms were analysed. We show the exposure map in Fig. 1, together with the positions of the 39 investigated DSGs. We used the maximum likelihood method to compare the measured data to models of celestial emission and background. In particular, the modelled time-patterns for each model component (see below) are fitted to the measured time-pattern of the data by maximising the likelihood of the data, i.e. estimating intensity scaling parameters for each sky and background component individually. In this maximum likelihood method, we account for photon count statistics being Poisson-distributed, and use the Cash statistic (Cash 1979) for measured data  $d_k$  and modelled data  $m_k = \sum_i \theta_i M_{ik}$  with model components  $M_{ik}$  for instrumental backgrounds and celestial signals (see Paper I for more details):

$$C(D|\theta_i) = 2 \sum_k [m_k - d_k \ln m_k], \quad (1)$$

where  $\theta_i$  are the individual intensity scaling parameters. By using the Cash statistic, the corresponding model  $m_k$  is positive definite in any case, avoiding an issue of negativity in data  $d_k$  that may occur if simple background subtraction would be applied instead. The goodness of fit for the baseline model was shown to be sufficient in Paper I.

Instrumental background is modelled by a self-consistent description of the data, treating instrumental line and continuum backgrounds separately (see Paper I). The focus of this work is to search for additional point-like 511 keV  $e^+e^-$  annihilation  $\gamma$ -ray signals beyond the diffuse large-scale emission. The overall emission from annihilating  $e^+$ s in the MW dominates the signal and hence a large scale emission model is needed to avoid possible falsely attributed emission. We adopt the large-scale emission model of Paper I which describes the Galaxy in 511 keV well through an empirical six-component model, made of 2D-Gaussians with different positions and sizes mapped onto the sky. In particular, this model consists of three extended components, which describe the inner Galaxy (narrow and broad bulge, respectively), and a thick low surface-brightness disk. Additionally, in the centre of the Galaxy, a point-like source is included (Skinner et al. 2014; Siegert et al. 2016). The two strongest continuum sources, the Crab and Cygnus X-1, are additional components of this model. We use these model components as a baseline model and superimpose the additional 39 DSGs, modelled as point-sources (see below), at their visible positions in the sky, while still allowing each baseline model components to vary in intensity, independently.

The background scaling parameters and the six celestial scaling parameters from Paper I were re-determined in the maximum likelihood parameter estimation to account for possible enhanced contributions from the DSGs.

### 2.2. Emission from Satellite Galaxies

The focus of our study is to search for 511 keV gamma-ray line signals which are produced when  $e^+$ s find  $e^-$ s to annihilate with<sup>1</sup>, either free or bound in atoms. The emissivity of 511 keV photons produced per unit time is driven by the annihilation conditions in the MW or in DSGs. These conditions include the number densities of  $e^+$ s and H-atoms as well as the ionisation fraction of H in the galactic ISM. While these number densities are large in the MW, there is no observational indication yet that there are similar large number densities in DSGs. This is unsurprising, as most of these objects contain only a small number of stars. In what follows, we nonetheless assume the number densities of H-atoms, or free electrons in the ISM of each dwarf galaxy to be large enough for each  $e^+$ -population to efficiently annihilate and produce a 511 keV line.

For simplicity, we assume the annihilation signals from DSGs to be point-like. If the signal is indeed from DM annihilation, the annihilation rate is proportional to the integral of the DM density squared over the line-of-sight (J-factor)

$$J \equiv \int_{\Delta\Omega} d\Omega \int_{l.o.s.} \rho^2 dl, \quad (2)$$

where the first integral is over the solid angle of the region of interest, and the second is over the line of sight, characterising

<sup>1</sup> When  $e^+$ s find  $e^-$ s, the resulting spectrum depends on the kinetic energies of the particles. Below a threshold of 6.8 eV,  $e^-$ s and  $e^+$ s can form an intermediate bound state, the positronium atom, which decays to either two 511 keV photons, or three continuum photons, distributed between 0 and 511 keV, see Ore & Powell (1949).

the distribution of annihilating DM in an astrophysical system. Typical dark matter density profiles follow a power law in the inner regions,  $\rho(r) \propto r^{-\gamma}$  (Burkert 1995; Navarro et al. 1996; Merritt et al. 2006) with  $0 < \gamma \leq 2$ . The  $\rho^2$  dependence of the J-factor thus yields a very sharply peaked signal, in most cases. Generally, compilations of dwarf galaxy J-factors in the literature (e.g. Ackermann et al. 2014; Evans et al. 2016) yield regions of interest that are smaller than the imaging resolution of SPI  $\sim 2.7^\circ$ , so that the point-like assumption is adequate. For example, the imaging resolution of SPI encompasses a physical region of more than 400 pc for the closest DSG in our sample, Canis Major (CMA), at a distance of 9 kpc.

Our input catalogue of all<sup>2</sup> DSGs near the MW within 500 kpc holds 39 individual candidate sources. We use the baryonic centres of the DSGs as the positions of the point-sources, see Tab. 1. This leads to 39 additional intensity scaling parameters  $\theta_i$  in the model fit to the observed data. These sources are at least separated by more than the imaging resolution of SPI ( $2.7^\circ$ ), and thus the correlation between them (source confusion) is usually negligible. Exceptionally "close pairs" (see Fig. 1) are CVn I – CVn II ( $6.5^\circ$ ), Leo I – Seg 1 ( $3.8^\circ$ ), Leo IV – Leo V ( $2.8^\circ$ ), and Boo I – Boo II ( $1.7^\circ$ ), so that the flux values derived from the latter pair only should be considered with caution.

For each galaxy, an individual spectrum in the range 490–530 keV was extracted. Then, in each spectrum, we determined the flux of annihilation emission separately. Due to the individually low signals, we additionally consider an alternative *stacking* approach for a DM hypothesis test. In this case, instead of deriving 39 individual spectra, we fix their relative fluxes according to their distances, assuming the same mass for all DSGs (Strigari et al. 2008a). This obtains a spectrum for a reference DSG at a chosen distance of  $D_0 = 100$  kpc. The resulting spectrum, however, would be dominated by the closest galaxy as the flux is proportional to the inverse distance squared, and may also be confused by the diffuse emission in the galactic plane and bulge, due to their partial correlation in the maximum likelihood approach. We try to avoid such a bias – in the stacking procedure only – by ignoring DSGs towards the galactic plane (between  $|b| < 10^\circ$ ), and galaxies closer than 25 kpc. Formally, the additional (now seventh, see Paper I) sky component is described by Eq. (3)

$$F = \frac{\langle L_0 \rangle}{4\pi D_0^2} \sum_{i=1}^{39} \delta(l - l_i) \delta(b - b_i) \left( \frac{D_0}{D_i} \right)^2. \quad (3)$$

Here  $\langle L_0 \rangle$  is the (fitted) intrinsic mean luminosity for a basic DSG at a canonical distance of  $D_0 = 100$  kpc, corresponding to 39 individual sources, at positions  $(l_i/b_i)$  in the sky, scaled by their distances  $D_i$ .

## 3. Results

### 3.1. Individual Sources

We first validate the emission attributed to the diffuse large-scale 511 keV emission to obtain a robust reference model with respect to possible additional sources. We find the bright bulge and faint disk, as well as the Galactic Centre Source (GCS), the Crab and Cygnus X-1 with fluxes consistent with the results reported in Paper I. The flux values for bulge, disk and GCS are  $(9.5 \pm 0.7) \times 10^{-4}$  ph cm<sup>-2</sup> s<sup>-1</sup>,  $(16.7 \pm 3.6) \times 10^{-4}$  ph cm<sup>-2</sup> s<sup>-1</sup>, and  $(0.8 \pm$

$0.2) \times 10^{-4}$  ph cm<sup>-2</sup> s<sup>-1</sup>, respectively. Continuum fluxes in the analysed 40 keV band are  $(2.20 \pm 0.07) \times 10^{-5}$  ph cm<sup>-2</sup> s<sup>-1</sup> keV<sup>-1</sup> for the Crab, and  $(0.65 \pm 0.05) \times 10^{-5}$  ph cm<sup>-2</sup> s<sup>-1</sup> keV<sup>-1</sup> for Cygnus X-1, also consistent with literature values (see e.g. Jourdain & Roques 2009; Jourdain et al. 2012).

The derived spectra for each DSG near 511 keV were fitted by a Gaussian-shaped line with width fixed at 2.15 keV (instrumental resolution, FWHM) on top of a constant offset. The centroid was allowed to vary in the range 508–514 keV, corresponding to bulk motions of  $|v_{Bulk}| \approx 1750$  km s<sup>-1</sup>, to account for intrinsic movement of the satellites and statistical fluctuations. For non-positive results, a  $2\sigma$  flux limit is estimated, for a line at 511 keV.

The strongest DSG signal that we find is from the position of Reticulum II (Ret II), with  $3.1\sigma$  significance. Its line flux is  $(17.0 \pm 5.4) \times 10^{-5}$  ph cm<sup>-2</sup> s<sup>-1</sup>. However, we caution that Ret II 511 keV emission may be too intense a signal to be interpreted as due to DM alone (see Discussion below). For the position of Sag, a 511 keV line significance of  $2.3\sigma$  is found. Formally, the line flux is  $(2.2 \pm 1.0) \times 10^{-5}$  ph cm<sup>-2</sup> s<sup>-1</sup>, consistent with the upper limits derived from Cordier et al. (2004), with a now  $\sim 100$  times larger exposure at this position.

The summary of fit results for all 39 tested satellite positions is listed in Tab. 1 and illustrated in Fig. 2. The exposure across the entire sky in this data set varies by a factor of 50 among the candidate sources, and the sensitivity changes accordingly. We empirically determine a  $2\sigma$  narrow 511 keV line detection sensitivity of  $5.7 \times 10^{-5} \times \sqrt{10^6/T_{Exp}[\text{Ms}]}$  ph cm<sup>-2</sup> s<sup>-1</sup> (solid line in Fig. 2). Among our sample of 39 candidate sources, 17 show weak indications of annihilation signals ( $\geq 1\sigma$ ), independent of the exposure time. Six sources show a signal with more than  $2\sigma$  (Leo I, Gru I, CVn II, Sag), and two sources more than  $3\sigma$  (Boo I, Ret II) statistical significance above instrumental background. The values for Boo I may be over-/underestimated due to source confusion with Boo II. Statistically, one would expect about two  $2\sigma$  sources out of a sample of 39 from fluctuations of the background. Since we see six sources at a significance of at least  $2\sigma$  (two expected), and 17 sources at a significance of at least  $1\sigma$  (13 expected), the 511 keV signals are not consistent with background fluctuations only. On the other hand, the individual 511 keV signals per source are of too low significance to single them out, and thus we will use the full population of possible sources for further analyses (see Sec. 4.1). Furthermore, we discuss the  $3.1\sigma$  signal from Ret II in Sec. 4.3, separately.

### 3.2. Stacked Analysis

Under the assumption that satellite galaxies share a common mass scale (Strigari et al. 2008a), we analyse the spectra in a constrained maximum likelihood fit to search for a DM-related 511 keV signal. For this, we determine one global scaling parameter to the set of sources, which are normalised to a common flux value and then re-scaled by their distances  $D^{-2}$ . We estimate the total  $\gamma$ -ray flux in the vicinity of 511 keV that reaches us from the positions of the Milky Way satellites (see Eq.(3)), and also avoid source confusion as above. In the stacked spectrum of the satellite galaxies at a canonical distance of 100 kpc, we do not find a significant excess and provide a  $2\sigma$  upper limit of the flux of  $1.4 \times 10^{-4}$  ph cm<sup>-2</sup> s<sup>-1</sup>. This is based on ignoring DSGs closer than 25 kpc and DSGs in the direction of the galactic disk. Softening these restrictions by including all 39 DSGs changes this upper limit to  $1.3 \times 10^{-4}$  ph cm<sup>-2</sup> s<sup>-1</sup>. If the assumption of an identical DSG mass is discarded, Eq. (3) gets an additional fac-

<sup>2</sup> During the write-up of this study, more DSGs have been found but have not been included in the analysis.

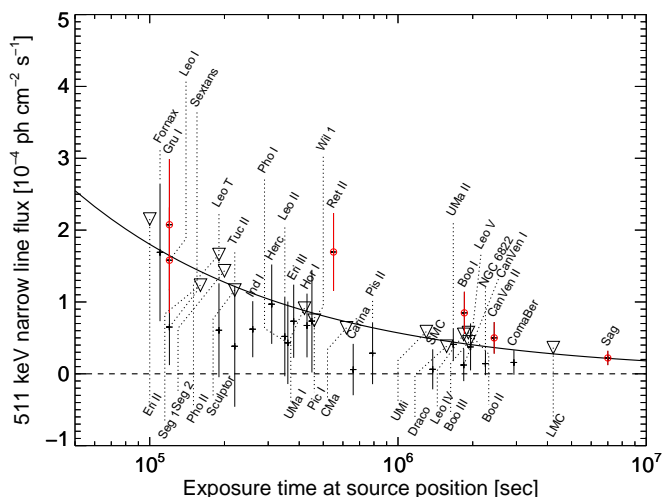


Fig. 2: Derived fluxes (crosses) of each satellite galaxy against the exposure time at source position. If a line is not detected or appears negative, a  $2\sigma$  upper limit is given (triangle). The solid line represents the  $2\sigma$  sensitivity limit for a narrow line (instrumental resolution) seen with SPI at 511 keV. The (red) circles indicate sources for which the statistical significance is higher than  $2\sigma$ .

for  $M_i^2$  where  $M_i$  is the dynamical mass of the DSG. For a subset of galaxies with available J-factor and dynamical mass estimates (see Tab. 1), we derive an upper limit of  $2.3 \times 10^{-4} \text{ ph cm}^{-2} \text{ s}^{-1}$ . Under the same assumptions, with the requirement that DM annihilation explains the entire bulge signal (Vincent et al. 2012; Evans et al. 2016), the stacked dark matter signal would yield a 511 keV flux of  $\sim 2 \times 10^{-6} \text{ ph cm}^{-2} \text{ s}^{-1}$ .

## 4. Discussion

### 4.1. Mass-to-Light-Ratios

The mass-to-light-ratio  $\Upsilon_V = M_{\text{dyn}}/L_V$  has been found to be a good indicator for DM which is believed to dominate the mass content in DSGs (Mateo 1998; Strigari et al. 2008a; McConnachie 2012). In the top-panel of Fig. 3, the mass-to-light ratio within the half-light radius (see references in Tab. 1) against the absolute V-band magnitude from available literature data is shown. For Pis II, Boo III, CMa, and the LMC, no dynamical mass estimate is available and we used the stellar masses as lower limits for the dynamical masses. As already shown by several studies (Mateo 1998; Strigari et al. 2008a; McConnachie 2012), the mass-to-light-ratio shows a negative correlation with the brightness of the objects. This is counter-intuitive as naturally one would expect a nearly constant mass-to-light-ratio in the absence of dark matter, no matter how faint a galaxy is. The stellar-mass-to-light-ratio  $\Upsilon_V^* = M^*/L_V$  indeed shows a value of  $\sim 1.0$  across the magnitude scale. But as the galaxies become fainter,  $\Upsilon_V$  rises, which indicates an unseen mass, generally interpreted as DM sub-halos. We note that also the ultra-faint dwarf galaxies (data available for Hor I and Ret II), recently detected by Koposov et al. (2015a), nicely fit into this correlation.

Any tracer that would make DM "visible", e.g. by measuring its annihilation products, should show a similar trend. We therefore define a mass-to-positron-annihilation-luminosity-ratio,  $\Upsilon_{511} = M_{\text{dyn}}/L_{511}$ , and calculate these values for our sample. In the bottom panel of Fig. 3, we show  $\Upsilon_{511}$  for the galaxies

whose flux estimates deviate from zero (at the  $1\sigma$  level). For all other galaxies for which data are available, we give  $2\sigma$  lower limits. Apparently, and although the data have large uncertainties, the correlation is opposite to  $\Upsilon_V$ . The reversed trend for  $\Upsilon_{511}$  versus  $M_V$  is in contradiction with what is expected for a DM origin. This could have several causes:

1. The correlation is based on the high ratio derived from Sag; by neglecting this value, the rank correlation coefficient reduces from  $-0.35$  to  $-0.14$ , but is still far from the positive correlation in the top panel. Using only signals with more than  $2\sigma$  does also yield the same correlation.
2. For the visually fainter galaxies (e.g. Ret II, Hor I) seen in 511 keV, the dynamical mass estimates are 2-3 orders of magnitude lower than for the bright galaxies (e.g. Sag, For) which automatically distorts the correlation in this direction, if the signals are not significant or strong.
3. It is probably not the dynamical mass which drives the apparent correlation: As the correlation of  $\Upsilon_V^*$  versus  $M_V$  is completely gone, the respective correlation between  $\Upsilon_{511}^*$  and  $M_V$  is still there. Stars and their surrounding environments are a favoured explanation for any present 511 keV emission (see discussion about Ret II below), though the electron number density in DSGs is a crucial but uncertain factor in theoretical estimations of the annihilation rate.

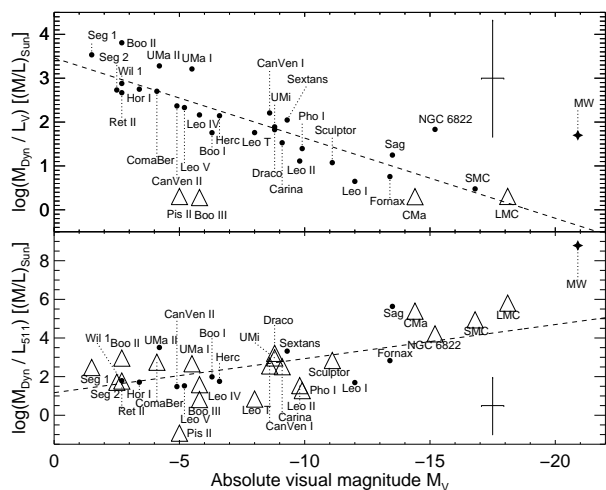


Fig. 3: Mass-to-luminosity ratio in units of solar masses per solar luminosity as a function of absolute visual magnitude,  $M_V$ . Top panel shows the dynamical mass over the absolute V-band magnitude as already described by Mateo (1998), Strigari et al. (2008a), or McConnachie (2012). Towards fainter satellite galaxies,  $\Upsilon_V$  increases, which is generally interpreted as indirect evidence for dark matter (see text for details). Bottom panel shows the ratio of the dynamical mass and the 511 keV luminosity over absolute visual magnitude. The trend is reversed when plotting  $\Upsilon_{511}$  versus  $M_V$ , in contradiction with what is expected for a dark matter origin. Typical error bars are shown;  $2\sigma$  lower limits are shown by triangles. For comparison,  $\Upsilon_V$  and  $\Upsilon_{511}$  for the Milky Way are shown with a star symbol in each panel.

### 4.2. Dark Matter Origin

The pronounced spatial peak of the 511 keV signal in the galactic centre has been confirmed and strengthened by recent results

(Paper I), reviving the possibility of a DM origin. If  $e^+$ s do not travel far from the source and rather find free or bound  $e^-$ s to annihilate with (Guessoum et al. 1991, 2005; Jean et al. 2009; Alexis et al. 2014), the morphology would match the square of a host galaxy's DM density profile (e.g. Burkert 1995; Navarro et al. 1996; Merritt et al. 2006). Interestingly, the peak of such a profile seen in 511 keV has been determined to be around  $(l/b) = (-1.25 / -0.25)^\circ$  (Kuhlen et al. 2013; Skinner et al. 2014). Vincent et al. (2012) found that Einasto profiles also fit the data well, assuming a DM halo centred on the galactic centre position. Upper limits on the 1-2 MeV  $\gamma$ -ray continuum (Boehm et al. 2004; Boehm & Silk 2008; Beacom & Yüksel 2006) limit the DM particle mass to  $m_{DM} \lesssim 7 \text{ MeV } c^{-2}$ . These studies also conclude that the morphology of the signal precludes a decay-induced signal.

In the case of the DSGs, the signal would be seen by SPI as a point-like source, and the 511 keV flux,  $F_{511}$ , would follow  $F_{511} = \frac{1}{4\pi} \frac{\langle\sigma v\rangle}{m_{DM}^2} J$ , assuming negligible positronium formation in the dwarfs, where  $\langle\sigma v\rangle$  is the thermally averaged cross section,  $m_{DM}$  is the DM particle mass, and  $J$  the J-factor, see Eq. (2). Hooper et al. (2004) estimated that if the whole 511 keV emission in the bulge of the MW was due to the annihilation of light DM particles into  $e^-e^+$ -pairs, an observable 511 keV emission from the direction of Sag would be about 3-6 times smaller than in the MW bulge. In our analysis, this ratio is  $42 \pm 19$ , ruling out this hypothesis by  $\sim 2\sigma$ , though it is worth pointing out that the flux ratio between the GCS and Sag is  $3.5 \pm 2.1$ . If the Sag signal is entirely due to DM, this would indicate a DM contribution to the galactic signal of  $\sim 3\%$ . However, more recent fits to the bulge emission require a DM annihilation cross section that is a factor of 5 (Ascasibar et al. 2006) to 10 (Vincent et al. 2012) times smaller. The updated J-factor for Draco (Ackermann et al. 2014; Evans et al. 2016) is furthermore  $\sim 5$  times smaller than what was used by Hooper et al. (2004). This may also apply to Sag, although its morphological structure is more complex due to tidal stripping. Overall, this means that our measurement of the Sag flux does little to constrain the galactic centre signal.

Based on available J-factors (Evans et al. 2016), and assuming in-situ positron annihilation and negligible positronium formation, the strongest constraint we obtain on a DM origin comes from Ursa Major II, due to its large J-factor. At  $2\sigma$  confidence level, we derive

$$\langle\sigma v\rangle < 5.6 \times 10^{-28} \left(\frac{m_{DM}}{\text{MeV}}\right)^2 \text{ cm}^3 \text{ s}^{-1}. \quad (4)$$

This constraint is still two order of magnitude above the cross section required to explain the entire MW bulge signal, and could be weakened even further if the density of interstellar gas is too low for  $e^+$ s to efficiently find partners to annihilate with.

### 4.3. Reticulum II

The ultra-faint dwarf galaxy Ret II (Koposov et al. 2015a; Simon et al. 2015) is found with a significance of  $3.1 \sigma$ . This is tantalising evidence for a bright source of positrons in Ret II, and among the other DSGs, Ret II might be special from the perspective of two different, maybe unrelated, measurements:

Ji et al. (2016) measured strong enhancements of neutron-capture elements in stars of Ret II, and interpret this as the result of nucleosynthesis of heavy elements from a single enrichment event only, which then would have to be a neutron star merger. The same enrichment event could be a positron source, e.g. through evolving into an accreting black hole system, or else

the existence of such neutron star binary also makes plausible the existence of a microquasar, producing  $e^+$ s in flaring states. On the other hand, there are suggestions for a star formation connection: Geringer-Sameth et al. (2015) reported a 2-10 GeV  $\gamma$ -rays with Fermi/LAT at  $2.3$  to  $3.7\sigma$  significance, and such  $\gamma$ -rays have been associated with star formation through cosmic-ray/gas interactions (Abdo et al. 2010; Ackermann et al. 2012, 2016). The effects of star formation are a non-negligible prerequisite for the 511 keV emission in the MW, as  $\beta^+$ -unstable radioactive nuclei are produced mainly in massive stars and their supernovae, and definitely contribute to the  $e^+$ -content in our Galaxy (see e.g. Diehl et al. 2006; Prantzos et al. 2011; Churazov et al. 2011; Alexis et al. 2014).

At a distance of 30 kpc, Ret II shows a present-day positron annihilation rate (assuming a positronium fraction of 1.0) of  $(3.7 \pm 1.2) \times 10^{43} \text{ e}^+ \text{ s}^{-1}$ . This value is at least as high as the one for the entire MW ( $(3.5 - 6.0) \times 10^{43} \text{ e}^+ \text{ s}^{-1}$ , see Paper I), and would support either the neutron star merger hypothesis of Ji et al. (2016) or the star formation picture of Geringer-Sameth et al. (2015). Either case may have produced a huge number of  $e^+$ s whose gradual, ongoing annihilation we now see in the ISM of Ret II.

Although the GeV excess in Ret II may also be attributed to DM particle annihilation, the Fermi/LAT data itself does not favour one or the other annihilation channel, because of the large uncertainty in the DM content (J-factor) of Ret II (Geringer-Sameth et al. 2015). Furthermore, Ret II and the LMC are the only DSGs that show a high-energy excess, disfavoured a DM explanation of the signal, as otherwise more DSGs should have been detected (Ackermann et al. 2014). Using the J-factors from Evans et al. (2016), a DM-only interpretation of the 511 keV signal from Ret II yields a cross section that would require a galactic bulge signal  $\sim 100$  times larger than observed. Indeed, this would indicate that at most  $\sim 1\%$  of Ret II's signal is due to DM annihilation.

## 5. Conclusion

We reported a search for 511 keV electron-positron annihilation emission from the satellite galaxies of the Milky Way within 500 kpc. Out of 39 tested sources, we find a signal from only one galaxy, Reticulum II, with a significance of  $3.1\sigma$ . The results for all other satellite galaxies are not in contradiction although not entirely consistent with statistical fluctuations of background. A combined (stacking) analysis of the satellite galaxies, assuming they share a common dark matter mass scale (Strigari et al. 2008a), also does not yield a positive signal, and we provide a  $2\sigma$  upper limit on the dark-matter related 511 keV line flux of  $1.4 \times 10^{-4} \text{ ph cm}^{-2} \text{ s}^{-1}$ . For a subset of galaxies with available masses and J-factors, we estimate a mass- and distance-weighted upper limit on the flux of  $2.3 \times 10^{-4} \text{ ph cm}^{-2} \text{ s}^{-1}$  (see included galaxies in Tab. 1). Even when we tentatively accept all marginal signals, the measured fluxes do not scale with the distances to the satellite galaxies. Furthermore, the closest satellite galaxy in our sample, Canis Major, does not show any signal ( $< 4.1 \times 10^{-5} \text{ ph cm}^{-2} \text{ s}^{-1}$  at  $2\sigma$ ), though it might be influenced by extended emission from the galactic plane.

We have established a firm upper limit on the 511 keV emission from a dark matter origin, though more sensitivity will be required to test the dark matter hypothesis as the origin of the signal. The case of Reticulum II and the 511 keV signal from this galaxy cannot entirely be attributed to dark matter; other origins related to star formation or a single neutron star merger (Geringer-Sameth et al. 2015; Ji et al. 2016), are thus more plausible

sible. Furthermore, we have used the constraints for the galactic centre 511 keV signal to show that the Reticulum II signal cannot be from dark matter alone. Understanding the signal of this dwarf galaxy may give clues about the true origin of the Milky Way bulge signal.

*Acknowledgements.* This research was supported by the German DFG cluster of excellence 'Origin and Structure of the Universe'. The INTEGRAL/SPI project has been completed under the responsibility and leadership of CNES; we are grateful to ASI, CEA, CNES, DLR, ESA, INTA, NASA and OSTC for support of this ESA space science mission. MGHK acknowledges funding via the Australian Research Council grant DE130101399.

## References

- Abdo, A. A., Ackermann, M., Ajello, M., et al. 2010, *ApJ*, 709, L152  
 Ackermann, M., Ajello, M., Allafort, A., et al. 2012, *ApJ*, 755, 164  
 Ackermann, M., Albert, A., Anderson, B., et al. 2014, *Phys. Rev. D*, 89, 042001  
 Ackermann, M., Albert, A., Atwood, W. B., et al. 2016, *A&A*, 586, A71  
 Alexis, A., Jean, P., Martin, P., & Ferrière, K. 2014, *A&A*, 564, A108  
 Ascasibar, Y., Jean, P., Bøhm, C., & Knödseder, J. 2006, *MNRAS*, 368, 1695  
 Battaglia, G., Tolstoy, E., Helmi, A., et al. 2011, *MNRAS*, 411, 1013  
 Beacom, J. F. & Yüksel, H. 2006, *Physical Review Letters*, 97, 071102  
 Bekki, K. & Stanimirović, S. 2009, *MNRAS*, 395, 342  
 Belokurov, V., Walker, M. G., Evans, N. W., et al. 2008, *ApJ*, 686, L83  
 Belokurov, V., Walker, M. G., Evans, N. W., et al. 2010, *ApJ*, 712, L103  
 Belokurov, V., Walker, M. G., Evans, N. W., et al. 2009, *MNRAS*, 397, 1748  
 Belokurov, V., Zucker, D. B., Evans, N. W., et al. 2007, *ApJ*, 654, 897  
 Belokurov, V., Zucker, D. B., Evans, N. W., et al. 2006, *ApJ*, 647, L111  
 Boehm, C., Hooper, D., Silk, J., Casse, M., & Paul, J. 2004, *Physical Review Letters*, 92, 101301  
 Bøhm, C. & Silk, J. 2008, *Physics Letters B*, 661, 287  
 Bouchet, L., Roques, J. P., & Jourdain, E. 2010, *ApJ*, 720, 1772  
 Burkert, A. 1995, *ApJ*, 447, L25  
 Caputo, F., Cassisi, S., Castellani, M., Marconi, G., & Santolamazza, P. 1999, *AJ*, 117, 2199  
 Carlin, J. L., Grillmair, C. J., Muñoz, R. R., Nidever, D. L., & Majewski, S. R. 2009, *ApJ*, 702, L9  
 Cash, W. 1979, *ApJ*, 228, 939  
 Churazov, E., Sazonov, S., Tsygankov, S., Sunyaev, R., & Varshalovich, D. 2011, *MNRAS*, 411, 1727  
 Clementini, G., Cignoni, M., Contreras Ramos, R., et al. 2012, *ApJ*, 756, 108  
 Coleman, M. G., Jordi, K., Rix, H.-W., Grebel, E. K., & Koch, A. 2007, *AJ*, 134, 138  
 Cordier, B., Attié, D., Cassé, M., et al. 2004, in *ESA Special Publication*, Vol. 552, 5th INTEGRAL Workshop on the INTEGRAL Universe, ed. V. Schoenfelder, G. Lichti, & C. Winkler, 581  
 Correnti, M., Bellazzini, M., & Ferraro, F. R. 2009, *MNRAS*, 397, L26  
 Cote, S., Freeman, K. C., Carignan, C., & Quinn, P. J. 1997, *AJ*, 114, 1313  
 Cotton, W. D., Condon, J. J., & Arbizzi, E. 1999, *ApJS*, 125, 409  
 Dall'Ora, M., Clementini, G., Kinemuchi, K., et al. 2006, *ApJ*, 653, L109  
 Dall'Ora, M., Kinemuchi, K., Ripepi, V., et al. 2012, *ApJ*, 752, 42  
 de Jong, J. T. A., Martin, N. F., Rix, H.-W., et al. 2010, *ApJ*, 710, 1664  
 de Jong, J. T. A., Rix, H.-W., Martin, N. F., et al. 2008, *AJ*, 135, 1361  
 Diehl, R., Halloin, H., Kretschmer, K., et al. 2006, *Nature*, 439, 45  
 Evans, N. W., Sanders, J. L., & Geringer-Sameth, A. 2016, *ArXiv e-prints*  
 Falco, E. E., Kurtz, M. J., Geller, M. J., et al. 1999, *PASP*, 111, 438  
 Feast, M. W. & Walker, A. R. 1987, *ARA&A*, 25, 345  
 Fellhauer, M., Evans, N. W., Belokurov, V., et al. 2007, *MNRAS*, 375, 1171  
 Fellhauer, M., Wilkinson, M. I., Evans, N. W., et al. 2008, *MNRAS*, 385, 1095  
 Gallart, C., Martínez-Delgado, D., Gómez-Flechoso, M. A., & Mateo, M. 2001, *AJ*, 121, 2572  
 Geringer-Sameth, A., Walker, M. G., Koushiappas, S. M., et al. 2015, *Physical Review Letters*, 115, 081101  
 Greivich, J. & Putman, M. E. 2009, *ApJ*, 696, 385  
 Grillmair, C. J. 2009, *ApJ*, 693, 1118  
 Guessoum, N., Jean, P., & Gillard, W. 2005, *A&A*, 436, 171  
 Guessoum, N., Ramaty, R., & Lingenfelter, R. E. 1991, *ApJ*, 378, 170  
 Gulliesz, M., Held, E. V., Rizzi, L., et al. 2008, *MNRAS*, 388, 1185  
 Guion, J. F., Hooper, D., & McElrath, B. 2006, *Phys. Rev. D*, 73, 015011  
 Hooper, D., Ferrer, F., Boehm, C., et al. 2004, *Physical Review Letters*, 93, 161302  
 Ibata, R. A., Gilmore, G., & Irwin, M. J. 1994, *Nature*, 370, 194  
 Irwin, M. J., Belokurov, V., Evans, N. W., et al. 2007, *ApJ*, 656, L13  
 Irwin, M. J., Bunclark, P. S., Bridgeland, M. T., & McMahon, R. G. 1990, *MNRAS*, 244, 16P  
 Jean, P., Gillard, W., Marcowith, A., & Ferrière, K. 2009, *A&A*, 508, 1099  
 Ji, A. P., Frebel, A., Chiti, A., & Simon, J. D. 2016, *Nature*, 531, 610  
 Jourdain, E. & Roques, J. P. 2009, *ApJ*, 704, 17  
 Jourdain, E., Roques, J. P., & Malzac, J. 2012, *ApJ*, 744, 64  
 Kirby, E. N., Simon, J. D., & Cohen, J. G. 2015, *ArXiv e-prints*  
 Kleyna, J. T., Wilkinson, M. I., Evans, N. W., & Gilmore, G. 2005, *ApJ*, 630, L141  
 Knödseder, J., Jean, P., Lonjou, V., et al. 2005, *A&A*, 441, 513  
 Koposov, S. E., Belokurov, V., Torrealba, G., & Evans, N. W. 2015a, *ApJ*, 805, 130  
 Koposov, S. E., Casey, A. R., Belokurov, V., et al. 2015b, *ArXiv e-prints*  
 Koribalski, B. S., Staveley-Smith, L., Kilborn, V. A., et al. 2004, *AJ*, 128, 16  
 Kraan-Korteweg, R. C. & Tammann, G. A. 1979, *Astronomische Nachrichten*, 300, 181  
 Kuhlen, M., Guedes, J., Pillepich, A., Madau, P., & Mayer, L. 2013, *ApJ*, 765, 10  
 Lee, M. G., Park, H. S., Park, J.-H., et al. 2003, *AJ*, 126, 2840  
 Leventhal, M., MacCallum, C. J., & Stang, P. D. 1978, *ApJ*, 225, L11  
 Majewski, S. R., Skrutskie, M. F., Weinberg, M. D., & Ostheimer, J. C. 2003, *ApJ*, 599, 1082  
 Martin, N. F., de Jong, J. T. A., & Rix, H.-W. 2008, *ApJ*, 684, 1075  
 Martin, N. F., Ibata, R. A., Bellazzini, M., et al. 2004, *MNRAS*, 348, 12  
 Martin, N. F., Ibata, R. A., Conn, B. C., et al. 2005, *MNRAS*, 362, 906  
 Mateo, M., Hurley-Keller, D., & Nemej, J. 1998, *AJ*, 115, 1856  
 Mateo, M. L. 1998, *ARA&A*, 36, 435  
 Matsunaga, N., Feast, M. W., & Soszyński, I. 2011, *MNRAS*, 413, 223  
 McConnachie, A. W. 2012, *AJ*, 144, 4  
 Merritt, D., Graham, A. W., Moore, B., Diemand, J., & Terzić, B. 2006, *AJ*, 132, 2685  
 Monaco, L., Bellazzini, M., Ferraro, F. R., & Pancino, E. 2004, *MNRAS*, 353, 874  
 Moster, B. P., Naab, T., & White, S. D. M. 2013, *MNRAS*, 428, 3121  
 Musella, I., Ripepi, V., Clementini, G., et al. 2009, *ApJ*, 695, L83  
 Musella, I., Ripepi, V., Marconi, M., et al. 2012, *ApJ*, 756, 121  
 Navarro, J. F., Frenk, C. S., & White, S. D. M. 1996, *ApJ*, 462, 563  
 Norris, J. E., Gilmore, G., Wyse, R. F. G., Yong, D., & Frebel, A. 2010, *ApJ*, 722, L104  
 Okamoto, S., Arimoto, N., Yamada, Y., & Onodera, M. 2008, *A&A*, 487, 103  
 Okamoto, S., Arimoto, N., Yamada, Y., & Onodera, M. 2012, *ApJ*, 744, 96  
 Ore, A. & Powell, J. L. 1949, *Physical Review*, 75, 1696  
 Peñarrubia, J., McConnachie, A., & Babul, A. 2006, *ApJ*, 650, L33  
 Piatek, S., Pryor, C., Bristow, P., et al. 2007, *AJ*, 133, 818  
 Picciotto, C. & Pospelov, M. 2005, *Physics Letters B*, 605, 15  
 Poretti, E., Clementini, G., Held, E. V., et al. 2008, *ApJ*, 685, 947  
 Pospelov, M., Ritz, A., & Voloshin, M. 2008, *Physics Letters B*, 662, 53  
 Prantzos, N., Boehm, C., Bykov, A. M., et al. 2011, *Reviews of Modern Physics*, 83, 1001  
 Queloz, D., Dubath, P., & Pasquini, L. 1995, *A&A*, 300, 31  
 Richter, O.-G., Tammann, G. A., & Huchtmeier, W. K. 1987, *A&A*, 171, 33  
 Rogstad, D. H., Rougoor, G. W., & Whiteoak, J. B. 1967, *ApJ*, 150, 9  
 Sand, D. J., Strader, J., Willman, B., et al. 2012, *ApJ*, 756, 79  
 Siegert, T., Diehl, R., Khachatryan, G., et al. 2016, *A&A*, 586, A84  
 Simon, J. D., Drlica-Wagner, A., Li, T. S., et al. 2015, *ApJ*, 808, 95  
 Simon, J. D. & Geha, M. 2007, *ApJ*, 670, 313  
 Simon, J. D., Geha, M., Minor, Q. E., et al. 2011, *ApJ*, 733, 46  
 Skinner, G., Diehl, R., Zhang, X., Bouchet, L., & Jean, P. 2014, in *Proceedings of the 10th INTEGRAL Workshop: "A Synergistic View of the High-Energy Sky"* (INTEGRAL 2014). 15-19 September 2014. Annapolis, MD, USA. Published online at <http://pos.sissa.it/cgi-bin/reader/conf.cgi?confid=228>, id.054, 054  
 Springel, V., White, S. D. M., Jenkins, A., et al. 2005, *Nature*, 435, 629  
 Strigari, L. E., Bullock, J. S., Kaplinghat, M., et al. 2008a, *Nature*, 454, 1096  
 Strigari, L. E., Koushiappas, S. M., Bullock, J. S., et al. 2008b, *ApJ*, 678, 614  
 The DES Collaboration, Bechtol, K., Drlica-Wagner, A., et al. 2015, *ArXiv e-prints*  
 Tyler, C. 2002, *Phys. Rev. D*, 66, 023509  
 Vedrenne, G., Roques, J.-P., Schönfelder, V., et al. 2003, *A&A*, 411, L63  
 Veljanoski, J., Ferguson, A. M. N., Mackey, A. D., et al. 2015, *MNRAS*, 452, 320  
 Vincent, A. C., Martin, P., & Cline, J. M. 2012, *J. Cosmology Astropart. Phys.*, 4, 022  
 Walker, M. G., Mateo, M., Olszewski, E. W., et al. 2015, *ApJ*, 808, 108  
 Walsh, S. M., Jerjen, H., & Willman, B. 2007, *ApJ*, 662, L83  
 Walsh, S. M., Willman, B., Sand, D., et al. 2008, *ApJ*, 688, 245  
 White, S. D. M. & Rees, M. J. 1978, *MNRAS*, 183, 341  
 Whiting, A. B., Hau, G. K. T., Irwin, M., & Verdugo, M. 2007, *AJ*, 133, 715  
 Willman, B., Blanton, M. R., West, A. A., et al. 2005a, *AJ*, 129, 2692  
 Willman, B., Dalcanton, J. J., Martínez-Delgado, D., et al. 2005b, *ApJ*, 626, L85  
 Willman, B., Geha, M., Strader, J., et al. 2011, *AJ*, 142, 128  
 Winkler, C., Courvoisier, T. J.-L., Di Cocco, G., et al. 2003, *A&A*, 411, L1  
 Young, L. M. 2000, *AJ*, 119, 188  
 Zaggia, S., Held, E. V., Sommariva, V., et al. 2011, in *EAS Publications Series*, Vol. 48, *EAS Publications Series*, ed. M. Koleva, P. Prugniel, & I. Vauglin, 215–216  
 Zucker, D. B., Belokurov, V., Evans, N. W., et al. 2006, *ApJ*, 643, L103

Table 1: List of Milky Way satellites tested for 511 keV emission, ordered by distance. The measured line flux  $F_{511}$  is given in  $10^{-5}$  ph cm $^{-2}$  s $^{-1}$ .  $M_{D_{dyn}}$  are the dynamical masses of the satellite in units of  $10^6 M_{\odot}$ ,  $M_V$  their absolute visual magnitude, and  $d$  the distance in kpc. The significance of a possible line detection is given in units of sigma.  $2\sigma$  or above detections are marked boldface. If a line is not present at all, a  $2\sigma$  upper limit on the flux is given. The positions of the assumed centres of the satellites are given in galactic longitude  $l$  and latitude  $b$  in units of degrees. The effective exposure time at the position of the sources  $T_{Exp}$  is given in Ms.  $M_{D_{dyn}}$ ,  $M_V$ ,  $d$ ,  $l$ , and  $b$  are taken from the literature (references, last column). The distances have been chosen as the given mean value from the NASA/IPAC Extragalactic Database (NED), if available.

| Name                                 | $d$        | $F_{511}$        | $M_{D_{dyn}}$ | $M_V$        | $\sigma$   | $l$           | $b$           | $T_{Exp}$   | Ref.                         |
|--------------------------------------|------------|------------------|---------------|--------------|------------|---------------|---------------|-------------|------------------------------|
| Canis Major <sup>b</sup>             | 9          | < 4.1            | > 49          | -14.4        | -          | 239.99        | -8.00         | 0.62        | (1),(16),(17)                |
| Segue 1 <sup>b</sup>                 | 23         | < 12.4           | 0.26          | -1.5         | -          | 220.48        | 50.43         | 0.16        | (1),(12),(60),(61),(62),(63) |
| <b>Sagittarius Dwarf</b>             | <b>28</b>  | <b>2.2(1.0)</b>  | <b>190</b>    | <b>-13.4</b> | <b>2.3</b> | <b>5.57</b>   | <b>-14.17</b> | <b>7.00</b> | (1),(44),(45),(46)           |
| <b>Reticulum II<sup>c</sup></b>      | <b>30</b>  | <b>17.0(5.4)</b> | <b>0.24</b>   | <b>-2.7</b>  | <b>3.1</b> | <b>266.30</b> | <b>-49.73</b> | <b>0.55</b> | (22),(23),(27),(42),(43)     |
| Ursa Major II <sup>c</sup>           | 34         | 4.1(2.3)         | 3.9           | -4.2         | 1.9        | 152.46        | 37.44         | 1.67        | (1),(57),(58),(59)           |
| Segue 2 <sup>c</sup>                 | 35         | < 14.4           | 0.23          | -2.5         | -          | 149.43        | -38.14        | 0.20        | (1),(48)                     |
| Willman 1 <sup>c</sup>               | 42         | 7.3(7.1)         | 0.39          | -2.7         | 1.0        | 158.58        | 56.78         | 0.45        | (1),(62),(64),(65)           |
| Coma Berenices <sup>c</sup>          | 44         | 1.6(1.7)         | 0.94          | -4.1         | 1.0        | 241.89        | 83.61         | 2.93        | (1),(6),(12),(18)            |
| Boötes III                           | 48         | < 4.4            | > 0.017       | -5.8         | -          | 35.41         | 75.35         | 1.93        | (1),(8),(9),(10)             |
| Boötes II <sup>a</sup>               | 49         | < 5.8            | 3.3           | -2.7         | -          | 353.69        | 68.87         | 1.92        | (1),(5),(6),(7)              |
| Large Magellanic Cloud               | 50         | < 3.6            | > 1500        | -18.1        | -          | 280.47        | -32.89        | 4.22        | (1),(37),(38)                |
| Tucana II <sup>c</sup>               | 57         | 3.8(8.4)         | N/A           | -3.8         | 0.5        | 328.08        | -52.32        | 0.22        | (22),(23)                    |
| Small Magellanic Cloud               | 61         | 0.6(2.8)         | 1400          | -16.8        | 0.2        | 302.80        | -44.30        | 1.38        | (1),(37),(52),(53)           |
| <b>Boötes I<sup>a,c</sup></b>        | <b>62</b>  | <b>8.5(2.9)</b>  | <b>0.81</b>   | <b>-6.3</b>  | <b>3.0</b> | <b>358.08</b> | <b>69.62</b>  | <b>1.85</b> | (1),(2),(3),(4)              |
| Ursa Minor <sup>c</sup>              | 73         | < 5.8            | 9.5           | -8.8         | -          | 104.97        | 44.80         | 1.30        | (1),(29)                     |
| Horologium I <sup>c</sup>            | 79         | 6.7(4.4)         | 0.55          | -3.4         | 1.6        | 271.39        | -54.73        | 0.43        | (22),(23),(27)               |
| Draco <sup>c</sup>                   | 82         | < 3.8            | 11            | -8.8         | -          | 86.37         | 34.72         | 1.57        | (1),(19),(20),(21)           |
| Phoenix II                           | 83         | < 16.6           | N/A           | -2.8         | -          | 323.68        | -59.75        | 0.19        | (22),(23)                    |
| Sculptor <sup>c</sup>                | 83         | < 11.6           | 14            | -11.1        | -          | 287.54        | -83.16        | 0.22        | (1),(47)                     |
| Sextans <sup>c</sup>                 | 85         | 6.5(5.3)         | 10.6          | -9.3         | 1.2        | 243.50        | 42.27         | 0.12        | (1),(49),(50),(51)           |
| Eridanus III                         | 87         | 7.3(5.1)         | N/A           | -2.0         | 1.5        | 274.95        | -59.60        | 0.38        | (22),(23)                    |
| Indus I                              | 100        | 6.2(3.9)         | N/A           | -3.5         | 1.6        | 347.15        | -42.07        | 0.26        | (23),(23)                    |
| Ursa Major I <sup>c</sup>            | 101        | < 9.2            | 11            | -5.5         | -          | 159.43        | 54.41         | 0.42        | (1),(6),(54),(55),(56)       |
| Carina <sup>c</sup>                  | 103        | 0.6(3.6)         | 6.3           | -9.1         | 0.2        | 260.11        | -22.22        | 0.66        | (1),(14),(15)                |
| Pictoris I                           | 114        | < 7.4            | N/A           | -3.1         | -          | 257.29        | -40.64        | 0.46        | (22),(23)                    |
| <b>Grus I<sup>c</sup></b>            | <b>120</b> | <b>20.8(9.1)</b> | <b>N/A</b>    | <b>-3.4</b>  | <b>2.3</b> | <b>338.68</b> | <b>-58.25</b> | <b>0.12</b> | (22),(23)                    |
| Hercules                             | 136        | 9.7(5.5)         | 2.6           | -6.6         | 1.8        | 28.73         | 36.87         | 0.31        | (1),(6),(12),(26)            |
| Fornax <sup>c</sup>                  | 139        | 16.9(9.6)        | 56            | -13.4        | 1.8        | 237.10        | -65.65        | 0.11        | (1),(24),(25)                |
| <b>Canes Venatici II<sup>c</sup></b> | <b>153</b> | <b>5.0(2.2)</b>  | <b>0.91</b>   | <b>-4.9</b>  | <b>2.3</b> | <b>113.58</b> | <b>82.70</b>  | <b>2.44</b> | (1),(6),(12),(13)            |
| Leo IV <sup>c</sup>                  | 155        | < 5.4            | 1.3           | -5.8         | -          | 265.44        | 56.51         | 1.84        | (1),(6),(12),(13)            |
| Pisces II <sup>c</sup>               | 182        | 2.9(4.3)         | > 0.0086      | -5.0         | 0.7        | 79.21         | -47.11        | 0.79        | (1),(39),(40),(41)           |
| Leo V <sup>c</sup>                   | 186        | 3.7(3.3)         | 1.1           | -5.2         | 1.1        | 261.86        | 58.54         | 1.96        | (1),(35),(36)                |
| Canes Venatici I <sup>c</sup>        | 216        | 1.2(2.2)         | 19            | -8.6         | 0.6        | 74.31         | 79.82         | 1.84        | (1),(6),(11)                 |
| Leo II <sup>c</sup>                  | 218        | 5.0(5.5)         | 4.6           | -9.8         | 0.9        | 220.17        | 67.23         | 0.35        | (1),(31),(32)                |
| <b>Leo I<sup>c</sup></b>             | <b>246</b> | <b>15.8(7.4)</b> | <b>12</b>     | <b>-12</b>   | <b>2.2</b> | <b>225.99</b> | <b>49.11</b>  | <b>0.12</b> | (1),(28),(29),(30)           |
| Eridanus II                          | 380        | < 21.6           | N/A           | -6.6         | -          | 249.78        | -51.65        | 0.10        | (22),(23)                    |
| Leo T <sup>c</sup>                   | 412        | 6.1(6.5)         | 3.9           | -8.0         | 1.0        | 214.85        | 43.66         | 0.19        | (1),(33),(34)                |
| Phoenix I                            | 418        | 4.3(5.7)         | 9.7           | -9.9         | 0.8        | 272.16        | -68.95        | 0.36        | (1),(66),(67),(68),(69)      |
| NGC 6822                             | 498        | 1.4(1.6)         | 3500          | -15.2        | 0.9        | 25.34         | -18.40        | 2.25        | (1),(29),(69),(70),(71),(72) |

**Notes.** (1) (McConnachie 2012), (2) (Belokurov et al. 2006), (3) (Fellhauer et al. 2008), (4) (Dall’Ora et al. 2006), (5) (Walsh et al. 2007), (6) (Grcevich & Putman 2009), (7) (Walsh et al. 2008), (8) (Grillmair 2009), (9) (Carlin et al. 2009), (10) (Correnti et al. 2009), (11) (Zucker et al. 2006), (12) (Belokurov et al. 2007), (13) (Okamoto et al. 2012), (14) (Kraan-Korteweg & Tammann 1979), (15) (Mateo et al. 1998), (16) (Martin et al. 2004), (17) (Martin et al. 2005), (18) (Musella et al. 2009), (19) (Cotton et al. 1999), (20) (Falco et al. 1999), (21) (Tyler 2002), (22) (Koposov et al. 2015a), (23) (The DES Collaboration et al. 2015), (24) (Piatek et al. 2007), (25) (Poretti et al. 2008), (26) (Musella et al. 2012), (27) (Koposov et al. 2015b), (28) (Whiting et al. 2007), (29) (Young 2000), (30) (Caputo et al. 1999), (31) (Coleman et al. 2007), (32) (Gullieuszik et al. 2008), (33) (Irwin et al. 2007), (34) (Clementini et al. 2012), (35) (Belokurov et al. 2008), (36) (de Jong et al. 2010), (37) (Richter et al. 1987), (38) (Feast & Walker 1987), (39) (Belokurov et al. 2010), (40) (Kirby et al. 2015), (41) (Sand et al. 2012), (42) (Simon et al. 2015), (43) (Walker et al. 2015), (44) (Majewski et al. 2003), (45) (Ibata et al. 1994), (46) (Monaco et al. 2004), (47) (Queloz et al. 1995), (48) (Belokurov et al. 2009), (49) (Irwin et al. 1990), (50) (Battaglia et al. 2011), (51) (Lee et al. 2003), (52) (Matsunaga et al. 2011), (53) (Bekki & Stanimirović 2009), (54) (Willman et al. 2005b), (55) (Kleyna et al. 2005), (56) (Okamoto et al. 2008), (57) (Peñarrubia et al. 2006), (58) (Fellhauer et al. 2007), (59) (Dall’Ora et al. 2012), (60) (Norris et al. 2010), (61) (de Jong et al. 2008), (62) (Martin et al. 2011), (63) (Simon et al. 2011), (64) (Willman et al. 2005a), (65) (Willman et al. 2011), (66) (Cote et al. 1997), (67) (Zaggia et al. 2011), (68) (Gallart et al. 2001), (69) (Mateo 1998), (70) (Koribalski et al. 2004), (71) (Rogstad et al. 1967), (72) (Veljanoski et al. 2015)<sup>(a)</sup> The values for Boo I may be over- or underestimated due to source confusion with Boo II, being not separated by at least one PSF. Likewise, the value for Boo II may be wrong, too. <sup>(b)</sup> For the stacking analysis, these galaxies have been ignored to validate the flux limit. <sup>(c)</sup> These galaxies have been included in the mass- and distance-weighted stacking analysis due to available dynamical mass and J-factor estimates, see Sect. 3.2.